

## Epitaxial relations, crystalline structure and defects in the double Si(111)/hR6 CaSi<sub>2</sub>/Si(111) heterostructures

N.G. Galkin<sup>1</sup>, S.A. Dotsenko<sup>1</sup>, K. N. Galkin<sup>1</sup>, L. Dózsa<sup>2</sup>, I. Cora<sup>2</sup>, B. Pécz<sup>2</sup>

<sup>1</sup>*Institute of Automation and Control Processes, Radio Str. 5, 690041 Vladivostok, Russia*

<sup>2</sup>*Institute of Technical Physics and Materials Research, Centre for Energy Research, Hungarian Academy of Sciences, 1525 Budapest Pf, 49, Hungary*

E-mail: galkin@iacp.dvo.ru

(Received August 26, 2016)

The morphology and crystalline structure of Si(111)/CaSi<sub>2</sub>/Si(111) double heterostructures (DHS) formed by the Ca reactive deposition epitaxy on the Si(111)7x7 surface and Si overgrowth at 500 °C have been studied by atomic force microscopy and transmission electron microscopy. It was established that stressed CaSi<sub>2</sub> layers with stacking faults in (001)CaSi<sub>2</sub> plane and {111}-twinned epitaxial or polycrystalline Si layers were grown. Epitaxial Si layers while had orientation parallel to the Si(111) substrate surface. CaSi<sub>2</sub>[100]||Si[1-10] and CaSi<sub>2</sub>(001)||Si(111) epitaxial relations were conserved for all grown DHS and they did not depend from the silicon growth mode: molecular beam epitaxy (MBE) or solid phase epitaxy (SPE). The CaSi<sub>2</sub> layer in (001)CaSi<sub>2</sub> plane has a hR6 modification and parameters:  $a=0.393\pm0.002$  nm;  $c=3.09\pm0.18$  nm at SPE Si growth mode. But some another parameters:  $a=0.382\pm0.002$  nm;  $c=3.09\pm0.18$  nm were observed at MBE Si growth mode. The compression in  $c$  parameter on near 1.07-1.14% as compared with  $c$ -value (3.06 nm) for tabular CaSi<sub>2</sub> data is established fact for both DHS. The observed differences in  $a$  parameter +1.85% (at SPE mode) and -1.08% (at MBE mode) is not clear now, and demands additional experiments. Some assumptions about mechanisms of occurrence and distribution of compressions and stretching in the CaSi<sub>2</sub> lattice were made.

### 1. Introduction

Two semiconductor compounds exist in Ca-Si system at atmospheric pressure: Ca<sub>2</sub>Si [1] and Ca<sub>3</sub>Si<sub>4</sub> [2]. It is known that CaSi<sub>2</sub> as a compound in the Ca-Si system with a maximum silicon concentration [1], it is a metal according to the theoretical work [3]. At atmospheric pressure a rhombohedral CaSi<sub>2</sub> structure with a space group R-3m and two modifications hR3 and hR6 has been observed [4]. The main problems for the CaSi<sub>2</sub> film's growth on Si substrate are the parameter mismatch of CaSi<sub>2</sub> and Si(111) crystal lattices (0.4-1.0%) [5] and near three-fold increase in CaSi<sub>2</sub> thermal expansion coefficient as compared with one for silicon at the growth temperature [6]. Therefore, after CaSi<sub>2</sub> film cooling to room temperature the lattice extension in the direction of [001] and compression in the direction of [100] were observed when the film thickness increases [6].

However, Ca silicide film grown at 500 °C on Si(111) substrate [7] was assigned to semiconducting Ca<sub>3</sub>Si<sub>4</sub>, since a transparency region in the photon energy range from 0.2 eV to 0.7 eV with band gap width of 0.63 eV and a plasma reflection region at energies less than 0.2 eV [7] were observed for them, which is typical for a degenerated semiconductor. Questions arise: does the film with Ca<sub>3</sub>Si<sub>4</sub> or stressed CaSi<sub>2</sub> composition is formed at 500 °C on Si(111) substrate and how the compression and stretching of the Ca silicide crystal lattice influence on the energy band structure of these films. Answering these questions is possible only after the simultaneous study of structure and properties of Ca silicide layers formed at 500 °C in the Si/Ca silicide/Si (111) DHS. The possible strong stresses in the CaSi<sub>2</sub> crystal lattice planes unrelated with epitaxial

CaSi<sub>2</sub>/Si(111) interface must be taken into account to.

In this work we only studied the peculiarities in the CaSi<sub>2</sub> crystalline structure, layer's morphology and defect formation in the cross sections of Si(111)/CaSi<sub>2</sub>/Si(111) double heterostructures (DHS) formed by Ca reactive deposition and then by silicon epitaxial overgrowth at the same temperature of 500 °C.

## 2. Experiment

Two series of samples were grown during growth experiments in the ultra-high vacuum "VARIAN" chamber with a base pressure  $2 \times 10^{-10}$  Torr. Rectangular Si strips (5x18 mm<sup>2</sup>) of p-type conductivity with resistivity 45 Ω·cm were used as substrates and Si sublimation sources. Two type of Si/Ca silicide/Si(111) DHS(s) were grown. The Ta-tube with small quantity of Ca (about 100 mg) was used as a Ca evaporation source with direct current heating. In both samples Ca and Si deposition rates, which calibrated by quartz sensor, were about (1.0-2.0) nm/min and 2.4 nm/min, correspondingly. In the first DHS the Ca silicide layer was grown by reactive deposition epitaxy (RDE) of 76 nm Ca layer thicknesses on an atomically clean Si(111)7x7 surface at 500 °C and then it was covered by Si top layer by method of molecular beam epitaxy (MBE) at 500 °C. In the second DHS the same Ca thicknesses (76 nm) was deposited by RDE method at 500 °C and covered by Si cap layer with 100 nm thickness at solid phase epitaxy (SPE) method at temperature of 500 °C.

The morphology of the Si/Ca silicide/Si heterostructures were studied by atomic force microscopy (AFM) using Solver P47 in tapping or contact mode immediately after re-loading of samples from growth chamber to reduce the influence of the oxidation on the film morphology.

A Philips CM 20 TEM at 200 keV was used to study cross-sectional specimens, and a JEOL 3010 HR TEM equipped with an energy filtering attachment (EFTEM) for elemental map's analysis (EELS) and the method of energy dispersive x-ray spectroscopy (EDX) was also applied. For the TEM study, the specimens were thinned by special procedure, which was explained in previous article [8], involving cutting with a diamond saw, embedding the pieces into a special titanium disk, mechanical grinding and polishing, and finally ion beam milling. Ar<sup>+</sup> ions of 10 keV energy were used until perforation, followed by low-energy (3 keV) milling to minimize surface damage. High resolution cross-section transmission electron microscopy (HR XTEM) images were studied for all grown double heterostructures. Selective area electron diffraction (SAED) patterns were registered for grown heterostructures, which promote the determination of epitaxial orientation for oriented films and heterostructures. A Selective Area Fast Fourier Transformations (SA FFT) of HR XTEM images were used for analysis of interplanar distances, its symmetry as compared with silicon substrate.

SA FFT patterns from HR XTEM images were analyzed using SingleCrystalTM and CrystalMaker® software [9]. Atomic force microscopy (AFM) images were analyzed with "Calculating of Average Parameters of Objects on Surface" software [10].

## 3. Results and discussion

After growth the morphology of Si/Ca silicide/Si(111) double heterostructures (DHS) were studied by atomic force microscopy method. The surface of both grown DHS(s) was unsmooth (Fig. 1(a,c)) that correspond to realization of island growth mechanism at the deposition of Ca atoms on Si(111)7x7 substrate and covering silicon layer atop Ca silicide layer formed on the first growth step by SPE or MBE methods. In the DHS with Si grown by SPE method (Fig. 1 a,b) the pinholes with density of  $1,3 \cdot 10^8$  cm<sup>-2</sup>, lateral sizes of 300-500 nm, their depth up to 20-30 nm and root mean square roughness of about  $\sigma_{\text{rms}} = 9.8 - 12.2$  nm were observed from height mode AFM image (Fig. 1 a). It was established that the pinhole depth is close to half of Si top layer thickness (40-45 nm). The AFM

phase mode image (Fig. 1 b) showed the silicon cap layer consists of grains (200-300 nm) with different orientation. Its form a near continuous layer, but have not cut. Both facts testify about polycrystalline nature of the Si top layer. The DHS with Si top layer grown by MBE method (Fig. 1c) was some smoother with  $\sigma_{\text{rms}} = 8.8 - 9.2$  nm, smaller density of pinholes of about  $(1-2) \cdot 10^7 \text{ cm}^{-2}$ , which have smaller sizes (100-300 nm) and the elongated form. Two phases with different contrast was found in the AFM phase mode (Fig. 1 d). They are located at different depths from the surface. The phase with a smaller contrast consists from large area and faceted silicon grains that correlate with its crystallization. The dipper ones have a stronger contrast and can be related to Ca silicide not covered by Si top layer or with very thin Si layer thickness atop. For this sample in the electron energy loss spectrum an interband transition at 6.2 eV and a small intensity of bulk plasmon at 14.6-14.8 eV, which are strongly differed from the Si ones, have been yearly observed [11]. So, really a Ca silicide grains are very close to the bottom of pinholes or the grains are on the surface in some places. The formation of deep pinholes confirms 3D mechanism of Si cap growth atop Ca

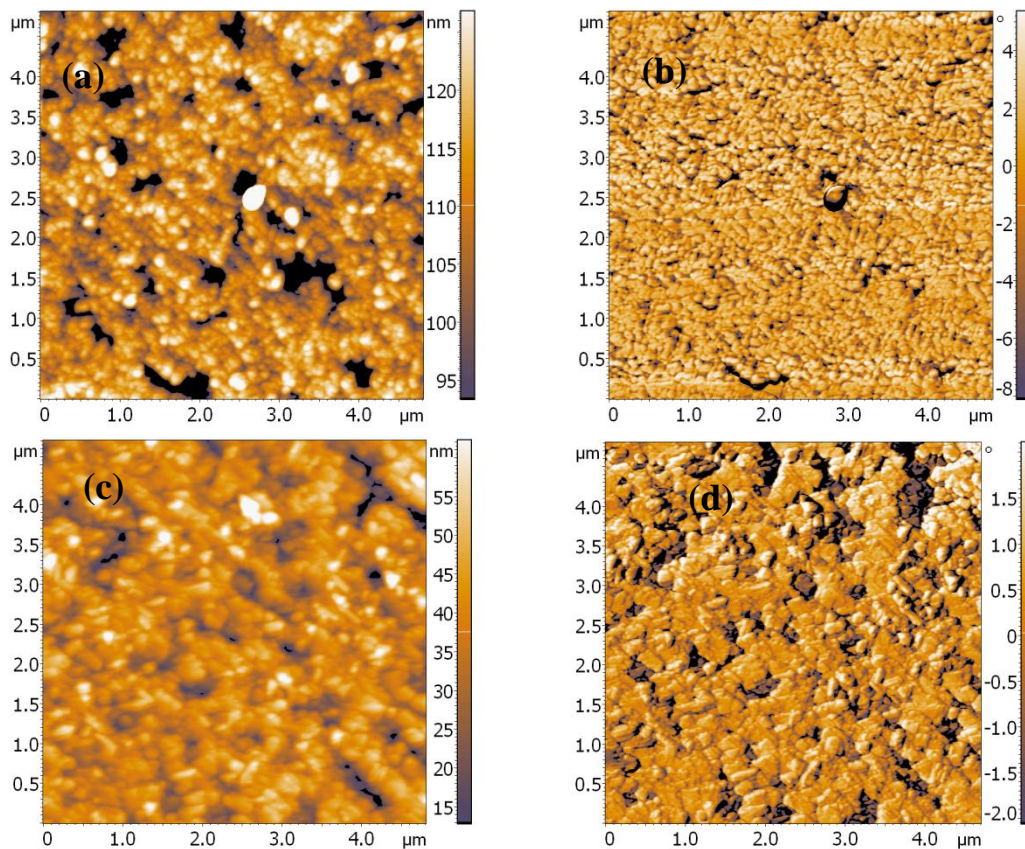


Fig. 1. AFM images of Si/Ca silicide/Si(111) DHS(s) with Si layer grown by SPE (sample V-445) (a,b) and MBE (sample V-442) (c,d) methods. Images *a* and *c* correspond to height mode, but images *b* and *d* – to phase mode.

silicide layer. Therefore, Ca silicide is mainly conserved inside silicon matrix at both DHS(s) with Si top layer grown by SPE and MBE methods. Morphology analysis of heterostructures showed that for the formation of continuous and smoother Si layer atop Ca silicide layer at given temperature we have to increase the silicon cap layer thickness both in MBE and SPE methods. The cutting of silicon grains was only observed in DHS with MBE grown silicon at 500 °C. But DHS real crystalline structure of Ca silicide, its orientation and composition can be transformed during the silicon capping layer growth at 500 °C. This situation depends from possibilities of epitaxial growth of Ca silicide on the Si(111) surface and silicon growth on the Ca silicide surface. Only cross section transmission



(50-70 nm instead 100 nm). What are the reasons of such a discrepancy? During the long time of the evaporator work (about 1 h for Ca) at fixed current across a Ta-tube the Ca calculated deposition rate can be decreased due to decrease of Ca mass in the evaporator. This leads to overestimation of calculated thickness and to increase of the experimental error in the determination of real Ca layer thickness. Additionally to the decrease of the Ca sticking coefficient to a silicon substrate at 500 °C must be taken into consideration. In the case of Si source the error value at the calculation of Si deposition rate could be increased due to the possible instability of the Ta-clamping contacts to Si plate in the home-made evaporator during its long work time (up to 30 min).

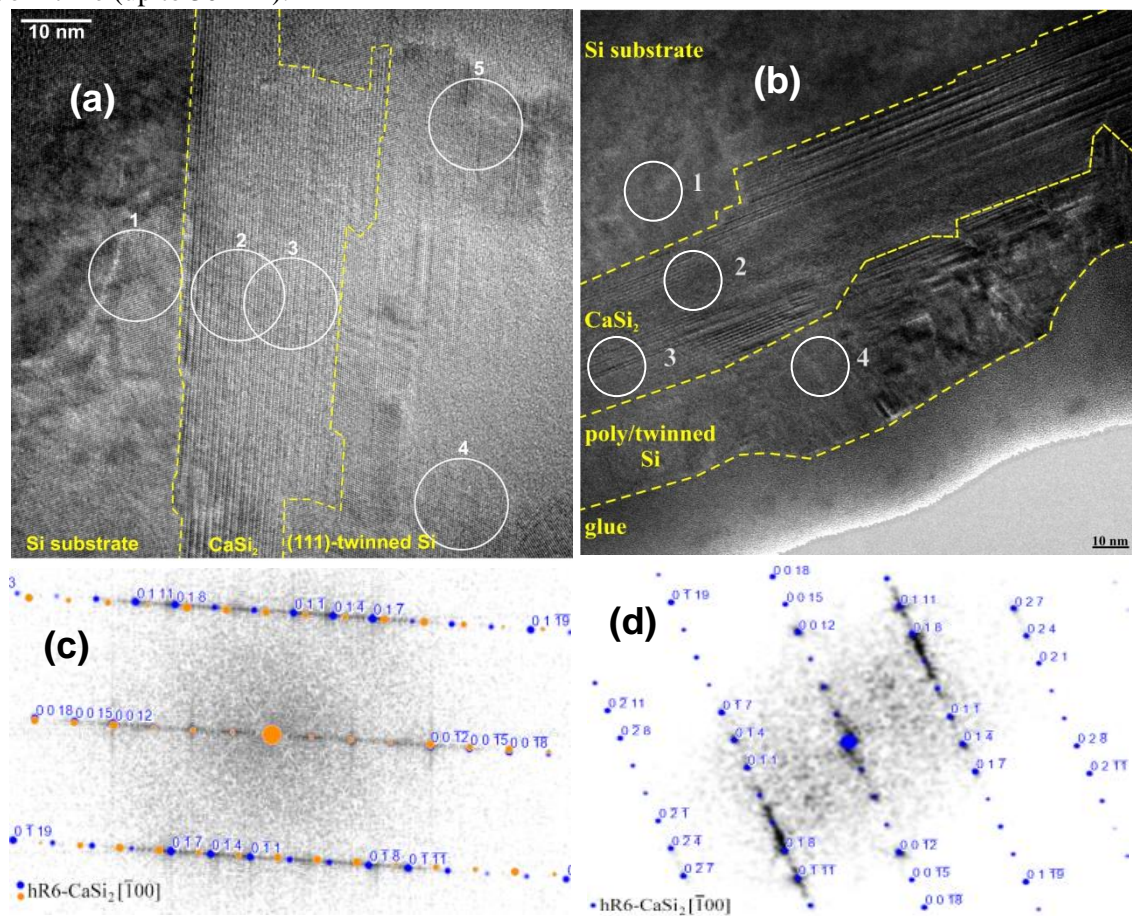


Fig. 3. HR XTEM images of the Si/hR-6  $\text{CaSi}_2$ /Si(111) DHS(s) with Si layers grown by SPE ((a), sample V-445) and MBE ((b), sample V-442) methods with inserts of white circles from 1 to 5 distributed in the DHS with Si and  $\text{CaSi}_2$  layers. SA FFT patterns from areas (2) on Fig. 3a and Fig. 3b with identification for  $\text{CaSi}_2$  planes in both DHS(s) with SPE Si mode (c) and MBE Si growth mode (d).

The SAED patterns from both DHS(s) (inserts on Fig. 2(a,b)) have proved the heteroepitaxial growth of the  $\text{CaSi}_2$  layer on Si(111) substrate independently from the silicon overgrowth regime (SPE or MBE) and non-abrupt  $\text{CaSi}_2$ /Si(111) interface. Besides, the thickness inhomogeneity in the  $\text{CaSi}_2$  and Si layers was observed from both XTEM data in BF regimes (Fig. 2(a,b)) and in DF regime (Fig. 2(c)) that correlated with valuable roughness by AFM data (Fig. 1(a,c)) for both samples. The DF image was acquired with the 006 reflection of the hR6-type  $\text{CaSi}_2$  phase. The  $\text{CaSi}_2$  and Si layers in the DHS with SPE (sample V-445) and MBE (sample V-442) grown Si are clearly separated (Fig. 2(a,b,c)).

Investigations of the structure, epitaxial relations and lattice parameters for both DHS(s) were carried out by analysis of HR TEM images and SA FFT patterns from different parts of double heterostructures, including interfaces,  $\text{CaSi}_2$  layer and Si top layer. HR TEM images for both DHS(s) are shown on Fig. 3(a,b). Different parts of the cross-section were marked by white circles, from which SA FFT patterns were created and then they were analyzed using SingleCrystalTM and CrystalMaker® software [9].

Based on the analysis of HR XTEM images for samples V-445 (Fig. 3 a) and V-442 (Fig. 3 b) it was shown that the  $\text{CaSi}_2$  epitaxial layer is firstly grown onto the (111)Si surface and then after the silicon overgrowth the double heterostructures are formed. Steps were observed on the Si(111) substrate – layer interfaces (Fig. 3 a,b). The  $\text{CaSi}_2$  layer and the Si top layer were not uniform in thickness that confirm a 3D island growth mechanism of  $\text{CaSi}_2$  film and non-uniform nucleation of Si atop  $\text{CaSi}_2$  layer.

Additional analysis of the Si/ $\text{CaSi}_2$ /Si(111) double heterostructure and its SA FFT patterns has shown the nearly flat the Si(111)/ $\text{CaSi}_2$  interface (Fig. 3(a), area (1)) with epitaxial relations:  $\text{hR6-CaSi}_2[100] \parallel \text{Si}[1-10]$  and  $\text{hR6-CaSi}_2(001) \parallel \text{Si}(111)$ . The identification of the SA FFT pattern for area (1) results in the un-defective  $\text{CaSi}_2$  layer growth on Si(111)7x7 surface without stacking faults in 3-4 unit cell thickness. But for larger  $\text{CaSi}_2$  distances from the Si(111) substrates few stacking faults of the Si sheets in the  $\text{CaSi}_2$  structure and twins were found by the identification of the SA FFT pattern (Fig. 3(a), right part of the area (2)). The  $\text{CaSi}_2$ /Si interface was studied for the area (3) on Fig. 3(a). The hR6-type  $\text{CaSi}_2$  layer ( $R\text{-}3\text{m}$ ;  $a=0.393\pm0.002$  nm;  $c=3.09\pm0.18$  nm) in [100] projection with stacking faults and the epitaxially grown {111}-twinned Si crystals (area 4) were found. Si crystals were epitaxially grown onto the (001) $\text{CaSi}_2$  surface (and the (111)Si surface of the substrate as well.). The epitaxial relations for the  $\text{CaSi}_2(001)$  on Si(111) substrate and near abrupt Si(111)/ $\text{CaSi}_2$  interface were conserved for Si/ $\text{CaSi}_2$ /Si DHS with MBE grown Si (Fig. 3 b, sample V-442, area 1). The stacking sequence was studied in the HR XTEM image for areas 2 and 3 (Fig. 3 b). It was established that in the first 5-10 nm thick part of hR6-type  $\text{CaSi}_2$  layer ( $R\text{-}3\text{m}$ ;  $a=0.382\pm0.002$  nm;  $c=3.09\pm0.18$  nm) a few stacking faults were observed. Afterwards  $\text{CaSi}_2$  sheets were grown without faults. In the upper and thinner part of the Si cap layer the {111}-twinned Si crystals were grown onto the  $\text{CaSi}_2(001)$  surface and the Si crystals are still oriented (area 4), i.e. one of the {111} planes is parallel to the Si(111) of the substrate. Mainly {111}-type twin boundaries and stacking faults are identified. The structural relationships and overlapping of the twinned Si-crystals are similar to the observations from the sample V-445.

A thorough analysis of the SA FFT patterns (Fig. 3 c, d) from the cross-sectional patterns of DHS(s) (samples V-445 and V-442) formed at 500 °C has shown that there are different deviations (stretching on 0.27-4.58 % and compression on 0.5-3.2%, Table 1) from tabular values for  $\text{CaSi}_2$  planes in the  $\text{CaSi}_2$  [-100] direction [12-14]. Simultaneously, 0.22-1.04% (compression) and 0.33-0.54% (stretching) was observed in the silicon lattice near the  $\text{CaSi}_2$ /Si interface (Table 2) that related to the difference in the lattice parameters [5] at growth and room temperatures. Calculations of the lattice parameters for embedded  $\text{CaSi}_2$  layers for both DHS(s) have shown (Table 3) that a rhombohedral  $\text{CaSi}_2$   $R\text{-}3\text{m}$  structure with hR6 modification has nearest values (with deviation in unit of percent) of the interplanar distances to tabular  $R\text{-}3\text{m}$   $\text{CaSi}_2$  ones [12] and their reflex's intensity. Therefore, it can be exactly concluded that grown DHS(s) have a  $\text{CaSi}_2$  composition with  $R\text{-}3\text{m}$  structure and hR6 modification, but not  $\text{Ca}_3\text{Si}_4$  as proposed in our first works [7,11,15].

The main difference in embedded  $\text{CaSi}_2$  layers was observed at change of the silicon growth method from SPE to the MBE. Lattice parameter  $c$  in the embedded  $\text{CaSi}_2$  layer is near the same for both samples and it is stretched as compared with tabular value (Table 3). But lattice parameter  $a$  in the embedded  $\text{CaSi}_2$  layer is stretched for V-445 sample (SPE) and compressed for V-442 sample (MBE). In addition different defects and stacking faults appear in some parts of  $\text{CaSi}_2$  embedded layer and Si cap layer by HR TEM data. These effects are not clear now and we only can discuss some possible reasons.

(i) The reason why on the Si(111)/CaSi<sub>2</sub> interface the heteroepitaxial growth is observed can be explained by good matching of CaSi<sub>2</sub>(100) and Si(111) planes due to intensive Ca and Si diffusion, including surface Si diffusion, on the beginning of Ca deposition on the atomically clean silicon surface. After the growth on near the continuous CaSi<sub>2</sub> layer the bulk diffusion of Ca and Si atoms is limited that results to the formation of stacking faults in CaSi<sub>2</sub> layer. Since the CaSi<sub>2</sub> layer thickness is non-homogenous due to competition of bulk and surface diffusion mechanisms, the second CaSi<sub>2</sub>/Si interface is not sharp too.

(ii) Alterations of CaSi<sub>2</sub> lattice constants along the interface also demands discussion. Different *a* CaSi<sub>2</sub> constants were observed in selected places of cross-sections (Fig. 3 a,b) for both samples (V-442 and V-445) as on the Si(111)/CaSi<sub>2</sub> and CaSi<sub>2</sub>/Si interfaces and in the center of embedded CaSi<sub>2</sub> layer. Since in both samples CaSi<sub>2</sub> was formed by RDE method at 500 °C, the parameter *a* of CaSi<sub>2</sub> lattice only depends from matching on the Si/CaSi<sub>2</sub> interface, temperature cooling regime and differences in Ca deposition rates. Ca deposition rates were distinguished only in two times: V-442 (2.0 nm/min) and V-445 (1.0 nm/min), so their cannot really influence on the difference in Si diffusion and lattice parameters at matching. But samples had the different cooling regimes. In the RDE/SPE sample (V-445) the CaSi<sub>2</sub> layer is cooled to room temperature before Si deposition with free CaSi<sub>2</sub> surface and can easily stretched to better matching to Si lattice. In the RDE/MBE sample (V-442) after the finishing of the growth procedure the formed Si/CaSi<sub>2</sub>/Si(111) DHS cooled to room temperature as a uniform system with different thermal expansion coefficients for Si and embedded CaSi<sub>2</sub> layer. The CaSi<sub>2</sub> surface was not free and can be compressed at influence of two silicon layers due to strong difference in the thermal expansion coefficient between CaSi<sub>2</sub> and Si [6].

(iii) Another fact is changing of *c* parameter of CaSi<sub>2</sub> lattice in different places of cross-sections for both samples. The difference in behavior at the interface depends mainly on the defect of CaSi<sub>2</sub> layer at the growth on silicon substrate. When growth takes place on a flat Si surface, the elastic matching of CaSi<sub>2</sub>(100) and Si(111) lattices without formation of stacking faults on depth of few nanometers is observed (Fig. 3 a). But at the CaSi<sub>2</sub> growth from the Si macro-step (up to 10 nm, Fig. 3 b)) the formation of stacking faults in CaSi<sub>2</sub> layer occur, what is the reason for the increase of *c* lattice constant of CaSi<sub>2</sub> and a noticeable change in its *a* constant. Since the interface is step mainly for V-442 sample, the main changes of CaSi<sub>2</sub> lattice constants are observed specifically for him. So, the crystalline quality of the first monolayers of CaSi<sub>2</sub> lattice in the [001] direction depends on sharpness of the Si(111)/CaSi<sub>2</sub>(100) interface and length of this region.

(iv) The third noticed fact is that with increased CaSi<sub>2</sub> layer thickness the CaSi<sub>2</sub> lattice defects on *c* parameter increases. We can propose that stacking faults at some distance from the Si(111)/CaSi<sub>2</sub>(100) interface are appeared due to limitation of Si diffusion flow from the Si substrate in the near continuous CaSi<sub>2</sub> film.

(v) An appearance of twinned Si planes can be explained by the low growth temperature

Table 1. Identifications of CaSi<sub>2</sub> planes in the CaSi<sub>2</sub>[-100] direction on SA FFT pattern for the V-445 and V-442 samples with Si/hr6 CaSi<sub>2</sub>/Si(111) DHS(s).

Planes in CaSi <sub>2</sub> [-100] direction	d <sub>CaSi<sub>2</sub></sub> (tab), [12] nm	d <sub>CaSi<sub>2</sub></sub> (V-445), nm	d <sub>CaSi<sub>2</sub></sub> (V-442), nm	Intensity [12], %	Δd/d, (V-445) %	Δd/d, (V-442) %
CaSi <sub>2</sub> (006)	0,5102	0,5114	0,5202	1,86	0,274	1,96
CaSi <sub>2</sub> (009)	0,3403	0,3289	0,3376	0,65	-3,261	-0,70
CaSi <sub>2</sub> (00 12)	0,2551	0,2579	0,2577	62,66	1,137	1,06
CaSi <sub>2</sub> (01-1)	0,3323	0,3384	0,3288	25,55	1,836	-1,05
CaSi <sub>2</sub> (01-4)	0,3053	0,3100	0,3203	43,39	1,201	4,58
CaSi <sub>2</sub> (01-7)	0,2555	0,2686	0,2609	100	1,152	2,10
CaSi <sub>2</sub> (018)	0,2517	0,2563	0,2507	43,13	1,823	0,40
CaSi <sub>2</sub> (01 11)	0,2138	0,2168	0,2127	57,33	1,389	-0,53

Table 2. Identifications of Si planes in the Si[1-10] direction on FFT pattern for the V445 sample with Si/CaSi<sub>2</sub>/Si(111) DHS.

Planes in Si[1-10] direction	d <sub>Si</sub> (tab), nm	d <sub>Si</sub> (V-445), nm	d <sub>Si</sub> (V-442), nm	Δd/d, V-445 %	Δd/d, (V-442) %
Si(002)	0,2715	0,27297	0,2712	0,54	-0,10
Si(111)	0,31356	0,31267	0,3146	-0,28	0,33
Si(220)	0,19201	0,19158	0,1900	-0,224	-1,04

Table 3. Calculation results for hR6-CaSi<sub>2</sub> lattice in the [-100] direction.

CaSi <sub>2</sub> lattice parameters, nm	V-445	V-442	bulk [12]	Δd/d, V-445 %	Δd/d, V-442 %	data errors, %
<b>a</b>	0,3931	0,3818	0,386	1,8508	-1,0784	±0,56
<b>c</b>	3,0949	3,0927	3,06	1,1417	1,069	±6,0

(500 °C) and sufficiently small Si diffusion coefficient as for SPE and for MBE Si growth methods. So, a nuclear of the silicon on the rough CaSi<sub>2</sub> surface occurs on different planes of the CaSi<sub>2</sub> epitaxial layer. When the CaSi<sub>2</sub> plane is smooth on some area, the silicon layer is epitaxially grown on such a surface. But when the different planes of CaSi<sub>2</sub> layer co-exist on the interface, the best growth is possible only on CaSi<sub>2</sub>(100) surface with small mismatch and on other CaSi<sub>2</sub> planes the weakly oriented Si growth with defects and twins can be observed. The last growth mechanism in the increasingly corresponds to the MBE growth of silicon capping layer and results to the formation of polycrystalline Si twinned layer.

(vi) The stress distribution along the length of the embedded CaSi<sub>2</sub> layer appears to be random. It depends on several factors: the presence of steps on the Si (111)/CaSi<sub>2</sub>(100) interface, compression or stretching the CaSi<sub>2</sub>(100) lattice parameter depending on the mode of Si growth (SPE or MBE), conditions of coalescence between CaSi<sub>2</sub> islands in the continuous CaSi<sub>2</sub> film and type of the formed defects, conditions of embedding and growth of silicon on the interface with CaSi<sub>2</sub> and other factors. The minimal compressions of *a* parameter and stretching of *c* parameter on about 1% on two interfaces and in the center of the film are observed at a thin CaSi<sub>2</sub> layer (Fig. 3 a, the upper part) in the sample V-445 (RDE/SPE). The stretching of *a* parameter up to 1.4 -1.8% and stretching of *c* parameter up to 0.6-1.8% increase on the thicker edge of CaSi<sub>2</sub> film. The first Si(111)/CaSi<sub>2</sub>(100) interface remains practically smooth without major steps. But steps are observed on the second interface with epitaxial Si layer in thicker silicide layer (Fig. 3 a, the lower part) that leads to appearance of stacking faults and to increase of *a* parameter. Parameter *c* is also increased in the step's area on the interface with epitaxial Si layer for sample V-442 (Fig. 3 b, the left part). The compression increase of *a* parameter is also observed that corresponds to the condition of existence of compression at the interface of CaSi<sub>2</sub> film with the silicon substrate. It can be assumed that the major factor, influencing on the stress distribution in CaSi<sub>2</sub> films are steps on the interfaces as with the substrate and the Si epitaxial layer, an appearance of which is associated with diffusion processes at the nucleation and growth of the Ca silicide film and Si on top of it.

#### 4. Conclusion

It was established that stressed CaSi<sub>2</sub> layers are formed at the reactive deposition epitaxy of Ca on the Si(111)7x7 surface at 500 °C, but at same temperature the {111}-twinned epitaxial or polycrystalline silicon capping layers were grown in the Si(111)/CaSi<sub>2</sub>(001)/Si(111) double heterostructures with conservation of the orientation relative to the substrate. The obtained epitaxial relations: CaSi<sub>2</sub>[100]||Si[1-10] and CaSi<sub>2</sub>(001)||Si(111) were conserved for CaSi<sub>2</sub> layers with a

thickness from 30 nm to 50 nm and they did not depend from the silicon growth mode (SPE or MBE at the temperature of 500°C). The formation of a sharp epitaxial interface was confirmed for grown DHS with formation in the silicon the embedded  $\text{CaSi}_2$  layer with hR6 modification and stressed parameters. For RDE/SPE sample was found parameters:  $a=0.393\pm0.002$  nm;  $c=3.09\pm0.18$  nm, but for RDE/MBE sample parameter  $c=3.09\pm0.18$  nm was conserved, but  $a=0.382\pm0.002$  nm was unexpectedly decreased that correspond to compression of the  $\text{CaSi}_2$  lattice at matching with Si(111) surface. The stretching of  $\text{CaSi}_2$  lattice  $a$  parameter with about per cent (1.07 - 1.14 %) in the (001) $\text{CaSi}_2$  plane with corresponding compression (0.22-1.04%) and stretching 0.33-0.54% of the silicon lattice parameters in (111)Si plane were confirmed near the Si(111)/ $\text{CaSi}_2$ (001) interface by HR TEM, SAED and SA FFT data. Grown DHS are interesting for optical and electrical investigations, which are in the progress.

## Acknowledgment

This work was carried out with financial support from the Russian Found of Basic Researches grant (No. 16-52-00074).

## References

- [1] D. B. Migas, L. Miglio, V. L. Shaposhnikov, and V. E. Borisenko, Phys. Rev. B **67**, 205203 (2003).
- [2] S. Lebegue, B. Arnaud, and M. Alouani, Phys. Rev. B **72**, 085103 (2005).
- [3] O. Bisi, L. Braikovich, C. Carbone, I. Lindau, A. Iandelli, G.L. Olcese, and A. Palenzona, Phys. Rev. B **40**, 10194 (1989).
- [4] P. Manfrinetti, M. L. Fornasini, and A. Palenzona, Intermetallics **8**, 223 (2000).
- [5] J. F. Morar and M. Wittmer, Phys. Rev. B. **37**, 2618 (1988).
- [6] G. Vogg, M. S. Brandt, M. Shutzmann, and M. Albrecht, J. Cryst. Growth **203**, 570 (1999).
- [7] S. A. Dotsenko, K. N. Galkin, D. A. Bezbabnyy, D. L. Goroshko, and N. G. Galkin, Phys. Procedia. **23**, 41 (2012).
- [8] A. Barna, B. Pecz, and M. Menyhard, Ultramicroscopy **70**, 161 (1998).
- [9] CrystalMaker Software Ltd and <http://www.crystallmaker.com> , (2016).
- [10] E. V. Sokolova, E. A. Chusovitin, A. O. Barabanova, S. A. Balagan, N. G. Galkin, and I.M. Yermak, Carbohydr. Polym. **93**, 458 (2013).
- [11] N. G. Galkin, D. A. Bezbabnyi, K. N. Galkin, S. A. Dotsenko, E. Zielony, R. Kudrawiec and J. Misiewicz, Phys. Status Solidi C **10**, 1819 (2013).
- [12] [http://www.icdd.com/products/technicalbulletins/Synchrotron\\_Neutron\\_Users\\_Guide.pdf](http://www.icdd.com/products/technicalbulletins/Synchrotron_Neutron_Users_Guide.pdf)
- [13] S. Fahy, D. R. Hamann, Phys. Rev. B **41**, 7587 (1990).
- [14] G. Vogg, M. S. Brandt, M. Shutzmann, M. Albrecht, J. Cryst. Growth **203**, 570 (1999).
- [15] N. G. Galkin, D. A. Bezbabnyi, S. A. Dotsenko, K. N. Galkin, I. M. Chernev, E. A. Chusovitin, P. Nemes-Incze, L. Dózsa, B. Pécz, T. S. Shamirzaev, and A. K. Gutakovski, Solid State Phenomena **213**, 71 (2014).